CrystEngComm

Accepted Manuscript

This is an *Accepted Manuscript*, which has been through the Royal Society of Chemistry peer review process and has been accepted for publication.

Accepted Manuscripts are published online shortly after acceptance, before technical editing, formatting and proof reading. Using this free service, authors can make their results available to the community, in citable form, before we publish the edited article. We will replace this *Accepted Manuscript* with the edited and formatted *Advance Article* as soon as it is available.

You can find more information about *Accepted Manuscripts* in the Information for Authors.

Please note that technical editing may introduce minor changes to the text and/or graphics, which may alter content. The journal's standard Terms & Conditions and the Ethical guidelines still apply. In no event shall the Royal Society of Chemistry be held responsible for any errors or omissions in this *Accepted Manuscript* or any consequences arising from the use of any information it contains.

ROYAL SOCIETY OF CHEMISTRY

www.rsc.org/crystengcomm

An effective route to the synthesis of carbonated apatite crystals with controllable morphologies and the growth mechanism†

Juan Shen,*[a] Jin Bo,[b] Ya-min Hu [a] and Qi-ying Jiang [a]

[a] *School of Materials Science and Engineering, Southwest University of Science and Technology, Mianyang 621010, China. E-mail: sj-shenjuan@163.com; Fax: +86 816 2419201; Tel: +86 816 2419201*

[b] *State Key Laboratory Cultivation Base for Nonmetal Composites and Functional Materials, Southwest University of Science and Technology, Mianyang 621010, China*

† Electronic supplementary information (ESI) available: XRD and FTIR analyses, additional TEM image, carbonate content calculation and solution chemistry calculation.

Carbonated hydroxyapatite (CHAp) powders with controllable morphologies and sizes were successfully synthesized *via* hydrothermal treatment by using hexamethylenetetramine (HMT) as a hydroxide anion-generating agent in a phosphate-surplus precursor solution. The products were characterized by X-ray diffraction, field emission scanning electron microscopy, energy-dispersive X-ray spectrometry, transmission electron microscopy, and selected area electron diffraction. Results revealed that the morphologies (such as micro-rods, sheet-like-assembled flowers, shaft wheel-like structures, bur-like spheres, dumbbell-shaped structures, and microspheres) of the products could be well tailored by regulating the reaction acidity and time. A possible growth mechanism accompanied with the effects of HMT on crystal nucleation and growth was preliminarily proposed for the formation of the controllable structures. This work indicated that the use of HMT as a hydroxide anion-adjusting agent is an effective strategy to finely control the morphology of CHAp crystals.

Introduction

The synthesis of nanocrystals with controllable shapes and sizes is significant in obtaining unique physical and chemical properties.[1] Controlling the crystal shape is important to understand the shape–property relationship and to develop functional materials for specific applications. Over the last few decades, excellent studies on the shape-controlled synthesis of inorganic crystals have been reported, such as rods,[2] wires,[3] flowers[4] and dendrites.[5] For example, several groups have fabricated hydroxyapatite [$Ca_{10}(PO_4)_6(OH)_2$, HAp] nanocrystals with various shapes *via* different wet chemical approaches (wet chemical precipitation,[6, 7] microemulsion,[8, 9] microwave irradiation,[10] and sonochemical method[11]) and investigated their shapes and sizes.

HAp is one of the most intensively investigated inorganic mineral materials. Given its chemical similarity to human bone and excellent biocompatibility, HAp is widely used as artificial bones[12] and catalysts,[13] as well as in drug delivery[14, 15] and environmental engineering.[16, 17] Numerous studies on the synthesis and characterization of HAp in solid state have been conducted over the past years. Most of the reported examples have focused on the development of HAp synthetic approaches toward size- and shape-controlled structures, such as nanoparticles,[9] nanorods,[18] whiskers/fibers/wires,[19] microspheres,[20] and mesoporous particles.[21] Lin et al. used calcium silicate as a precursor and obtained HAp with controllable morphologies and chemical compositions by adopting a hydrothermal route.[22] Ito et al. found that dicalcium phosphate is a suitable precursor to control HAp crystal structures through a solution-phase pathway.[23] Uniform nanorods of HAp with an unusual orthorhombic shape were also synthesized in the presence of gelatin and $CO(NH_2)_2$. Zhan et al. found that a single-crystal-to-single-crystal top chemical transformation may be attributed to the evolution of HAp nanorods from the precursor octacalcium phosphate [$Ca_8(HPO_4)_2(PO_4)_4 \cdot 5H_2O$, OCP] phase.[24] Although many kinds of morphologies have been investigated for HAp, studies on the alkaline source to control HAp crystal structures are

CrystEngComm Accepted Manuscript

limited and the mechanism of nucleation and crystal growth of HAp crystals are not completely elucidated.

In this paper, we present micro-rods, sheet-like-assembled flowers, shaft wheel-like structures, bur-like spheres, dumbbell-shaped structures, and microspheres of carbonated HAp (CHAp) crystals obtained *via* hydrothermal process. In contrast to previous studies that employed $NH_3 \cdot H_2O$ or NaOH to adjust the solution pH, the present study introduces hexamethylenetetramine (HMT) as a hydroxide anion-generating agent to gradually increase the solution pH at a controlled rate in a phosphate-surplus solution (Ca/P ratio = 0.67 precursor solution). The synthesis of HAp product with shaft wheel-like structures is rarely reported. Therefore, we successfully synthesize the CHAp powders with unique three dimensional architectures *via* a simple and effective approach. The formation mechanisms of the shaft wheel-like structures and the effects of HMT on crystal nucleation and growth are also discussed.

Experimental Section

Synthesis. In a typical process, $CaCl_2$ (0.01 mol) and ethylenediaminetetraacetic acid (EDTA) (0.01 mol) were dissolved in 100 mL of hot distilled water. When the solution became clear, 0.0152 mol of Na_2HPO_4 and 0.02 mol of HMT were gradually mixed into the solution with vigorous stirring. Drops of 6 M HCl or NaOH solution were added to adjust the pH to different values. The mixture solution was concentrated to 100 mL, transferred into a Teflon-lined stainless steel autoclave, and maintained at 190 °C for 4 h. After the reaction was completed, the solid precipitate was filtered and washed several times with distilled water, and the obtained powders were dried in a lyophilizer.

Characterization. X-ray diffraction (XRD) analysis was performed using an X'Pert PRO X-ray diffractometer with Cu Kα radiation. The 2θ range used was from 3° to 60° with a speed of 4°/min. Fourier transform infrared (FT-IR) spectra (KBr pellets) were obtained using a Nicolet-6700 FT-IR spectrometer. Field emission scanning electron microscopy (FESEM) images were obtained with a Zeiss Ultra 55 scanning electron microscope at an accelerating voltage of 15 kV. Elemental analysis was conducted by using an Oxford X-Max 50 energy-dispersive X-ray spectrometer, which was directly connected to the scanning electron microscope. High-resolution transmission electron microscopy (HRTEM) and electron diffraction were performed using a Zeiss Libra 200FE transmission electron microscope at an accelerating voltage of 200 kV. The samples for transmission electron microscopy (TEM) were prepared by dispersing powdered CHAp products on carbon-coated Cu grids. The Brunauer–Emmett–Teller (BET) surface area was quantified by measuring the N_2 adsorption–desorption isotherms by using a Micromeritics Tristar 3000 porosimeter.

Results and Discussion

In our research, the hydroxide anion-generating agent is the key factor in fabricating different forms of crystalline CHAp and is the unique aspect of our study compared with previous reports.[25] When the alkaline source is supplied by NaOH or ammonia–water instead of HMT, the products show different morphologies. NaOH or ammonia–water rapidly provides hydroxide anions because of its strong basicity. When NaOH acts as the alkaline source, samples exhibit needle-like, whisker-like and plate-like structures, and their width is in a large size range.[26] Zhu et al, used KOH and ammonia–water to adjust the pH value of reaction solution, and obtained prism-like morphology HAp crystals with well crystallinity and a relatively large size.[27] When $NH_3 \cdot H_2O$ is chosen as the alkaline source, nonuniform morphologies are found and there is a distribution of small particles and large agglomerates.[28] However, during the chemical reaction at a high temperature, OH^- is supplied by HMT in a homogeneous gradual process, and the generation rate of HAp nanoparticles is slow in the solution. The relatively slow generation rate of HAp is favorable for the subsequent growth of various crystal structures along the determined direction. HMT, as a pH buffer, can function as a slow release source of OH^- ions (simplified reactions (1) and (2)), and the release behavior is consistent with the observed long-term pH of the reactive

CrystEngComm Accepted Manuscript

solution (Fig. 1).[29]

$$(CH_2)_6N_4 + 6H_2O \rightarrow 4NH_3 + 6HCHO \quad (1)$$

$$NH_3 + H_2O \rightarrow NH_4^+ + OH^- \quad (2)$$

The pH value decreased from 10 to 30 min starting from pH values higher than 6.1. This decrease is due to the consumption of OH^-: (i) during the transition from $Ca_8H_2(PO_4)_6(H_2O)_5$ (OCP) to $Ca_{10}(PO_4)_6(OH)_2$ (HAp), the H_3PO_4 production can decrease the reaction solution pH, as shown in the simplified reactions (3) and (4) for the formation of the HAp phase. The X-ray diffraction (XRD) pattern (Fig. S1, ESI†) of CHAp sample obtained after 30 min, 1 h and 4 h with initial pH 8.1 indicate the presence of OCP as transient precursor. Fig. S1A, ESI† displays the characteristic diffraction reflections of OCP phase (JCPDS card: No. 26-1056). By increasing the hydrothermal time up to 1 h the major part of the sample was composed of hydroxyapatite crystals most probably coming from the OCP hydrolysis (Fig. S1, ESI†).

$$8Ca^{2+} + 8HPO_4^{2-} + 5H_2O \rightarrow Ca_8H_2(PO_4)_6(H_2O)_5 + 2H_3PO_4 \quad (3)$$

$$Ca_8H_2(PO_4)_6(H_2O)_5 + 8H_2O \rightarrow 4Ca_{10}H_2(PO_4)_6(H_2O)_2 + 6H_3PO_4 \quad (4)$$

(ii) Given the initial basicity of the solution, the dissolution and ionization of CO_2 became more active, whereas the action of NH_3 was suppressed (simplified reactions (5) and (6)). An acidic carbonate-anion-rich solution was then formed. [30]

$$CO_2 + 2OH^- \rightarrow CO_3^{2-} + H_2O \quad (5)$$

$$NH_3 + H_2O \rightarrow NH_4^+ + OH^- \quad (6)$$

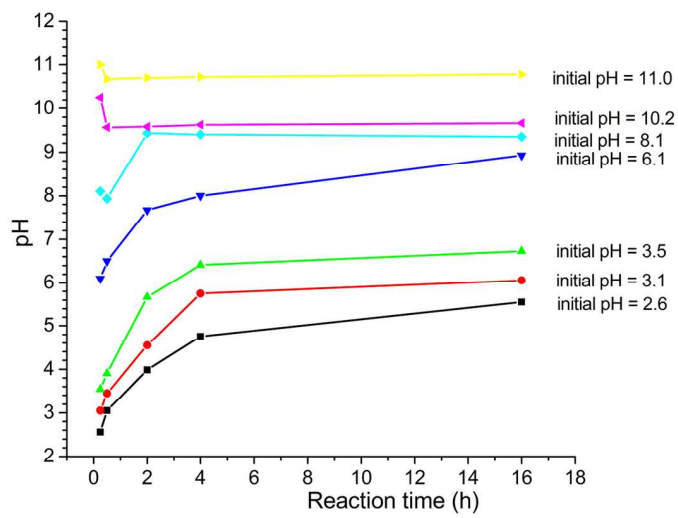

Fig. 1 pH values of growth solution measured after hydrothermal reaction for 10 min, 30 min, 2 h, 4 h, and 16 h to as-prepared CHAp samples synthesized with different initial pH values.

Figure S2, ESI† shows the activity evolution versus pH of the main calcium, EDTA, and phosphate species and ion pairs in the mother solution in the pH range between 3.5 and 11.0. The data shown in Figure S2, ESI† were generated at 100 °C due to the temperature limit of the modelling software. Hence, the activity values are not the actual experimental values but provide a trend for the activity. Figure S2, ESI† shows that the Ca-EDTA complex ($CaEDTA^{-2}$) tends to stabilize with the pH increase. The activity of the ionic $CaH_2PO_4^+$ pair was higher at lower pH and it decreased when increasing the pH, which may be EDTA caused a decrease in free calcium ions in solution. However, the activity of the $CaPO_4^-$ pair increased with the pH. It should be noted that previous studies on HAp precipitation had identified the calcium phosphate pair as the CaP growth units.[31, 32] The saturation index of the calcium phosphate (CaP) phases as a function of pH (Table S1, ESI†) shows that SI(HAp) increases with the pH. The data of SI(OCP) showed a trend of first increase and then decrease. According to the classical theory of nucleation the increase of supersaturation produced a decrease of the nucleation activation energy and consequently an increase of the nucleation rate may occur.[33, 34] For the system under study, the increase of

CrystEngComm Accepted Manuscript

SI(HAp) with increasing pH may explain the burst of a larger number of HAp nuclei rather than the other CaP phases at higher pH values.

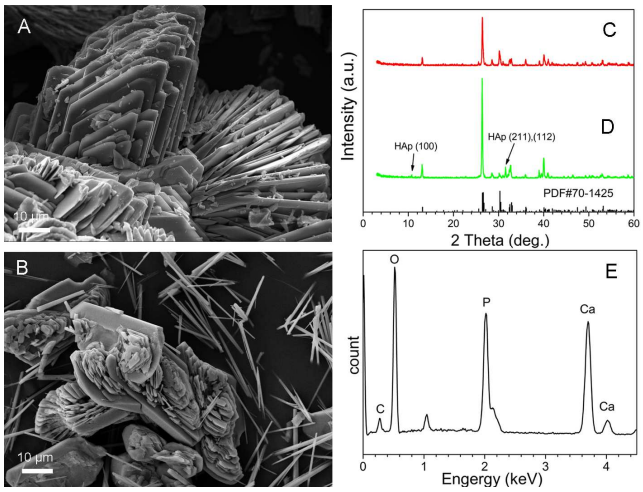

Fig. 2 Scanning electron microscopy images of as-prepared CHAp samples synthesized at 190 °C for 4 h with different initial pH values: (A) pH = 2.6 and (B) pH = 3.1; XRD patterns of samples synthesized at 190 °C for 4 h with different initial pH values: (C) pH = 2.6 and (D) pH = 3.1 and the standard data of brushite (JCPDS No. 70-1425) as a reference; (E) energy-dispersive X-ray spectrum of a rod-shaped crystal in Fig. 2B.

The chemical composition of the precursor solution had a Ca/P ratio of 0.67 (lower than the stoichiometric value), which indicates the presence of an excess amount of phosphates in the apatite crystal forms. The product was dicalcium phosphate anhydrous ($CaHPO_4$, DCP) at lower pH, and the obtained morphologies were dependent on the Ca/P ratio. Fig. 2 shows FESEM images and XRD patterns of the samples prepared at initial pH values of 2.6 and 3.1 with hydrothermal treatment at 190 °C for 4 h. At the experimental conditions shown in Fig. 2A, neatly arranged platelet crystals were produced. When the pH value was increased, platelets and rod crystals were observed (Fig. 2B). The samples were sequentially analyzed *via* XRD. The product prepared at an initial pH of 2.6 was identified as the DCP phase (JCPDS card: No. 70-1425). The sample prepared under initial pH 3.1 is identified as the mixture of DCP and HAp phases (JCPDS card: No. 09-0432). The energy-dispersive X-ray spectrometry pattern is shown in Fig. 2E. The Ca/P ratio of 1.5 indicates that the rod-like product was probably composed of Ca-deficient apatite because the Ca/P ratio of HAp was 1.67. It could be present the transition from DCP to HAp with hydrolysis occurred in an alkali solution.

The XRD patterns (Fig. S3, ESI†) of the CHAp samples at various initial pH conditions (keeping the ratio of Ca/P as 0.67) show similarity to those of $Ca_5(PO_4)_3OH$ (JCPDS card: No. 09-0432). The diffraction peaks of the five samples can be indexed as a pure hexagonal phase with space group *P*63/*m* (176), which coincides well with the standard data for the HAp phase. A significant difference was observed in the relative intensities based on the (002), (211), and (300) peaks for the five samples in the XRD patterns. This result indicates the possibility of different preferential orientation growths at different pH conditions.

The FT-IR spectra of CHAp prepared at different pH values are shown in Fig. S4, ESI†. The band at around 3570 cm^{-1} was assigned to the stretching vibration of the hydroxyl group. From Fig. S4A, the characteristic hydroxyl group band of HAp at 3570 cm^{-1} (νOH) was not clearly visible. The intensity of the hydroxyl group band gradually became strong when the pH values were increased above 3.5 because a considerable amount of OH^- can enter the hexagonal crystal lattice with increasing pH value (Figs. S4B–E, ESI†). The wide absorption bands at around 3426 and 1633 cm^{-1} were attributed to the adsorbed water. The broad and weak bimodal peaks at 1466 (ν_3) and 1406 (ν_3) cm^{-1} were attributed to the carbonate ion in the B-site, which indicates the replacement of some PO_4^{3-} ions by CO_3^{2-} ions.[35] The peaks at 1091 (ν_3), 1023 (ν_3), 963(ν_1), 606 (ν_4), and 565 cm^{-1} (ν_4) were the characteristic bands for PO_4^{3-}. Therefore, the FT-IR spectra indicate that all the as-synthesized samples were

CrystEngComm Accepted Manuscript

CO_3^{2-}-substituted apatite crystal. A quantitative analysis of the carbonate content was carried out based on the FTIR spectra (Table S2, ESI†). Featherstone et al. reported that the extinction ratio was a function of carbonate content, the calculated carbonate contents were about 1.88–3.28 *wt*% in all CHAp samples.[36] The result shows that the crystals incorporated more carbonate and hydroxyl ions at a high pH than those at a low pH. The increase in CO_3^{2-} substitution to a particular extent was possibly due to the presence of CO_2 from the atmosphere.

Fig. 3 shows the typical FESEM images of CHAp powders prepared at 190 °C at various initial pH values. Various 3D hierarchical superstructures of CHAp were synthesized simply by adjusting the pH value. Significant differences existed in the morphology and crystallite sizes of CHAp powders. The CHAp powder prepared at pH 3.5 was composed of microrods with about 10–20 μm in length and 0.5–1 μm in diameter in Fig. 3A. A hexagonal prism composed of hexagonal prismatic units was arranged in parallel (Fig. 3B). When the pH was increased from 3.5 to 6.1, a uniform 3D-structured flower-like product was observed (Fig. 3C). The diameter of the obtained flowers was about 10–25 μm, and the flowers consisted of 2D nanosheets. The high-magnification image shows that the nanosheet had a thickness of about 20–50 nm, widths of 1–3 μm and lengths up to 2 μm, and almost no particles or rods were observed (Fig. 3D). When the pH was increased to 8.1, shaft wheel-like structures of self-assembled high-aspect-ratio micro-sheets (lengths up to 3 μm and widths of 300–500 nm) were obtained in Figs. 3E and 3F. The powder prepared at pH 10.2 was composed of bur-like microspheres of self-assembled nanorods (Figs. 3G and 3H). At pH 11.0, dumbbell-shaped structures and microspheres of self-assembled nanorods were obtained. The high-magnification image in Fig. 3J shows that the microrod crystals grew out of small nanorod crystals *via* the splitting. Consequently, the overall morphology changed from 1D microrods to 3D hierarchical superstructures when the pH was increased from 3.5 to 11.0. Therefore, pH is an important factor in controlling CHAp with various morphologies.

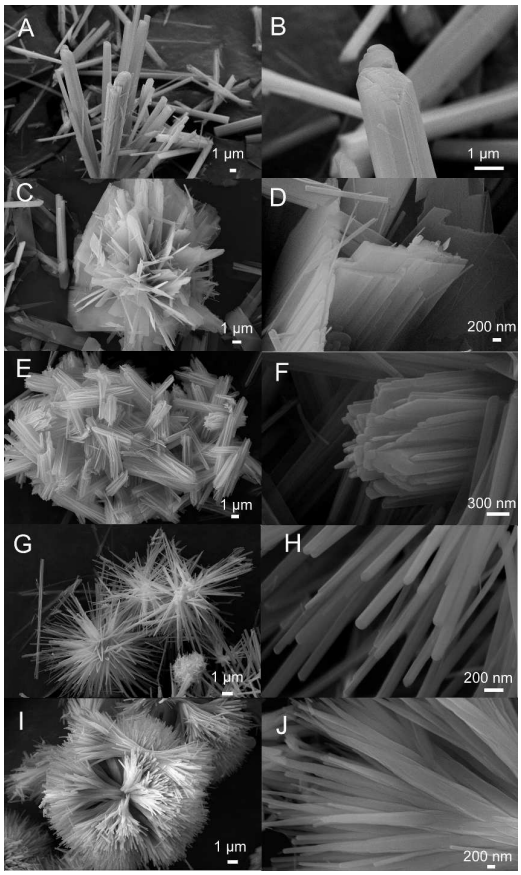

Fig. 3 FESEM images of as-prepared CHAp samples synthesized at 190 °C for 4 h with different initial pH values: (A, B) pH = 3.5, (C, D) pH = 6.1, (E, F) pH = 8.1, (G, H) pH = 10.2, and (I, J) pH = 11.0.

CrystEngComm Accepted Manuscript

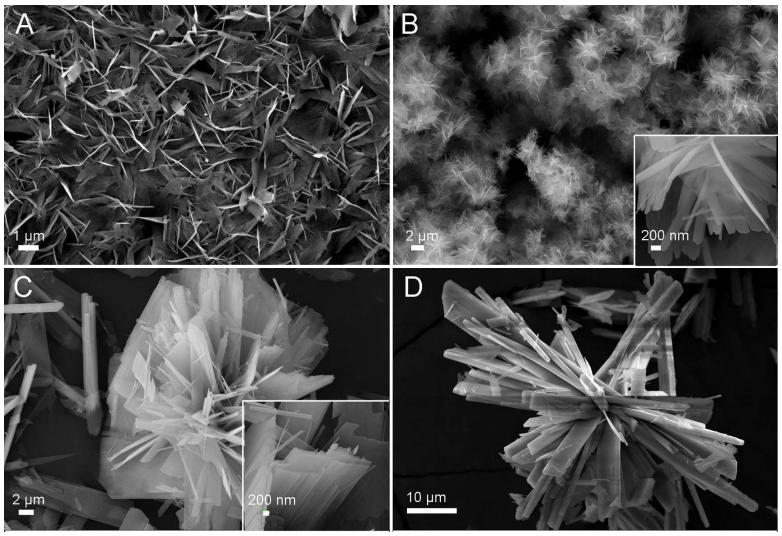

Fig. 4 FESEM images of CHAp samples synthesized at 190 °C with pH = 6.1 and at different reaction times: (A) 10 min, (B) 30 min, (C) 4 h, and (D) 16 h.

In this work, several time-dependent hydrothermal experiments were conducted to investigate the growth mechanism of various CHAp structures. The size and morphology of the samples prepared at 190 °C for 10 min, 30 min, 4 h, and 16 h with an initial pH value 6.1 were characterized *via* FESEM (Fig. 4). After 10 min of hydrothermal treatment, only a small amount of the product was obtained. As shown in Fig. 4A, the morphology of the as-produced samples in the early stage had a willow-like shape with a thickness of about 100 nm, widths of 100–300 nm and lengths of 500–800 nm. When the hydrothermal time was increased to 30 min, these sheets assembled into flower-like structures (Fig. 4B). When the reaction time was further increased to 4 h, the flowers grew wider, longer, and thicker than those in Fig. 4B. The morphology of the final product is shown in Fig. 4D. Thick sheets were assembled into flower clusters. The arrow shows a typical hexagonal shape at the sheet end. Figs. 4A–D shows the process of self-assembling growth from a willow-like to flower-like morphology.

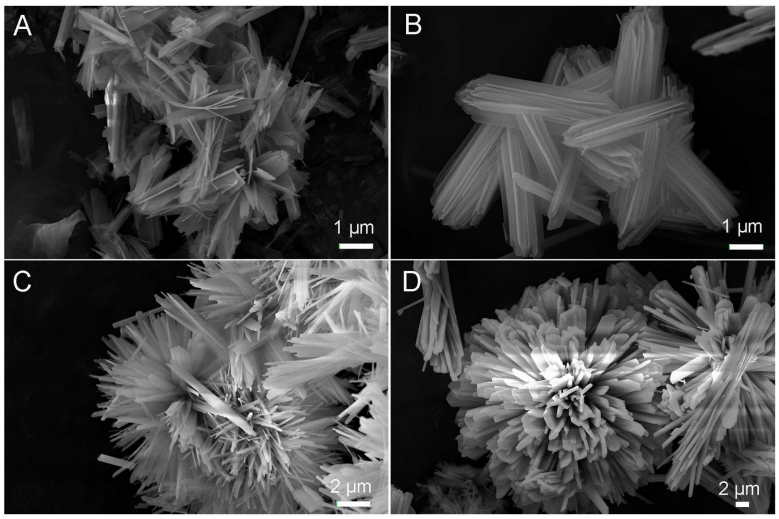

Fig. 5 FESEM images of CHAp samples synthesized at 190 °C with pH = 8.1 and at different reaction times: (A) 30 min, (B) 4 h, (C) 16 h, and (D) 24 h.

CrystEngComm Accepted Manuscript

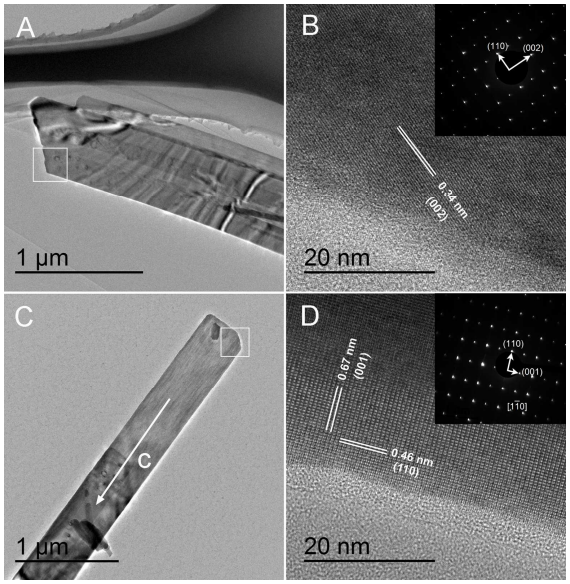

Fig. 6 TEM (A, C) and HRTEM (B, D) images of CHAp powders synthesized at 190 °C with pH = 8.1 for 4 h and 16h, respectively. Insets: corresponding SEAD patterns.

The apatite products were obtained after hydrothermal treatment at 190 °C for 30 min, 4 h, and 16 h with an initial pH value 8.1. The size and morphology of the samples were characterized via FESEM to investigate the formation mechanism of the 3D structured apatite flowers (Fig. 5). In Fig. 5A, the as-prepared product had a sheet-like shape with widths of 300–700 nm and lengths up to 800 nm at a hydrothermal reaction time of 30 min. The sheets underwent lateral aggregation to form shaft wheel-like-structured CHAp. When the hydrothermal treatment time was increased to 4 h, the sheets grew longer and more orderly than those in Fig. 5A. The BET surface area was 46 m^2/g, which is a relatively high value. Materials with these unique structure characteristics and high surface areas can be potentially used in catalyst and water treatment.[13, 37] When the reaction time was above 16 h, the sheet-like crystals radiated from a central nucleus assemble into flower-like structures (Figs. 5C and 5D).

Fig. 6 shows the TEM and HRTEM images and the corresponding selected area electron diffraction (SAED) (top right insets) images of individual apatite sheets (from Figs. 5B and 5C). The samples obtained at reaction times of 4 and 16 h displayed the same crystal structures. The HRTEM image shows the lattice fringes with interplanar spacings of 0.34 nm which correspond to the (002) plane of HAp (Fig. 6B), and the preferential growth direction was along the *c*-axis of the hexagonal HAp. The HRTEM image in Fig. 6D shows that the fringe spacings of a single nanosheet were 0.46 and 0.67 nm, which correspond to crystal planes (110) and (001). The discrete SAED spots demonstrate that the synthetic apatite sheets are well-crystallized hexagonal single crystals.[38]

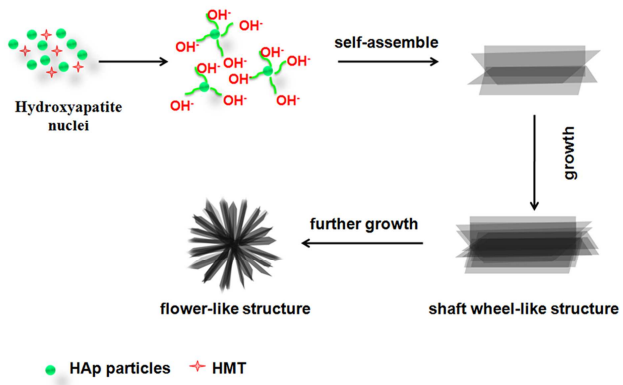

Fig. 7 Scheme illustration of a possible formation mechanism of 3D-structured CHAp flowers.

CrystEngComm Accepted Manuscript

The formation mechanism of the 3D-structured CHAp flower crystal is proposed based on the experimental results, as shown in Fig. 7. The experimental results indicate that the entire formation process includes nucleation, growth of sheet-like crystals, and self-assembly growth. Normally, HAp has different crystallographic planes ({100} and {001} planes). HAp columnar structures bound by six (100) facets are grown along the *c* axis, which leads to the formation of HAp rods. However, platy forms were produced at a relatively high pH even at the hydrothermal condition. Adding HMT into the reaction solution was favorable for the formation of nanosheet HAp crystal mainly at the earlier stage of crystal growth (Fig. 5A) maybe because the growth of *c*-surfaces was limited, whereas the growth of the *a*, *b*-surfaces was enhanced. Thus, HAp nanosheets were obtained, and this result is in agreement with the XRD results (Fig. S3C, ESI†). The nanosheet HAp crystal was observed by Kobayashi et al. in a supersaturated solution system based on SBF.[39] Lin, et al used urea as the homogeneous precipitation reagent and obtained a product with a nanosheet morphology.[40] In the presence of HMT, the formation of the nanosheet HAp nanocrystallites facilitated aggregation parallel to the *c* axis. The side-by-side sheet-like structure along the *c* axis grew in an orderly manner based on the FESEM and TEM micrographs (Figs. 5B and S5, ESI†). Given the high surface energy of the nanocrystals, the newly formed HAp sheets were organized in a specific orientation to reduce their surface energy as the reaction time progressed. In this way, the final product was a 3D-structured CHAp flower, which was formed by the sheet-like crystals radiating from a central nucleus.

The FESEM images of the products prepared at specific reaction time intervals with an initial pH value of 11.0 are shown in Fig. 8. The formation process includes nucleation, splitting growth, and formation of microspheres. When the reaction time was short, the crystals were bundle-like particles. This morphology is symmetric to the long axis. Based on the experimental results, at higher pH, the anisotropy of surface charge distribution could be caused by the adsorption of hydroxide ions onto preferential crystal facets, which had a strong effect on the formation of particular particle shapes via oriented aggregation of the primary particles.[10] When the reaction time was increased, the bundle-like particles grew and split at the end of the broom-like crystals. This phenomenon differs from the dumbbell-like growth reported in a double-diffusion system.[41, 42] When the reaction time was further increased, HAp microspheres were obtained.

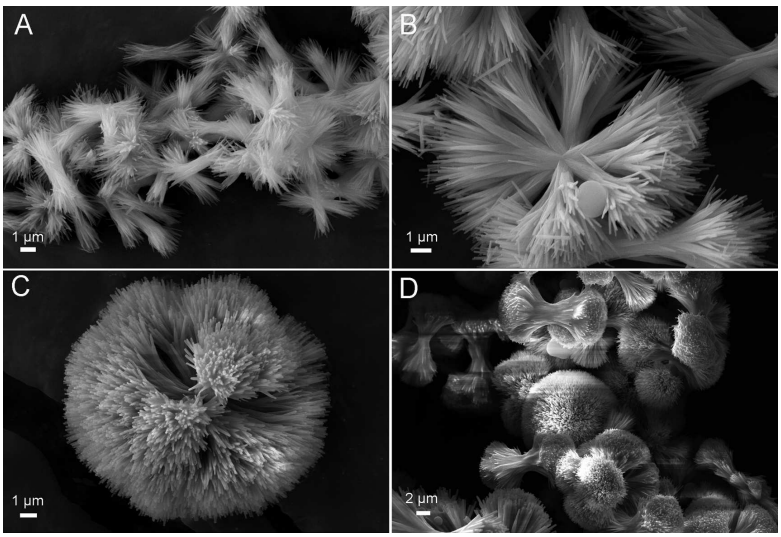

Fig. 8 FESEM images of CHAp samples synthesized at 190 °C with pH = 11.0 and at different reaction times: (A) 30 min, (B) 2 h, (C) 4 h, and (B) 16 h.

In principle, crystal growth and crystal morphology were determined by various extrinsic and intrinsic factors, such as solution pH value, the degree of supersaturation, chelating reagent and the crystallographic phase of the nucleated seeds. In this paper, the pH value is an important factor that influences the precipitation of apatite phase from aqueous solutions. The main morphologies of the CHAp samples are governed by solution pH value (HMT

CrystEngComm Accepted Manuscript

as alkaline source in this paper). In addition, the relationship between the distribution of pH value and the supersaturation degree of the reaction system may also have important functions in the formation of the different morphologies of CHAp crystals. According to the calculated SI values at different pH values (Table S1, ESI†), the formation of CHAp with different morphologies (shown by representative FESEM images) are possible with different supersaturation levels. Olson, et al. synthesized fluorapatite nanostructures with various shapes (prismatic, ellipsoidal, star, and aggregate) and found that their structures are correlated with the supersaturation of the system.[43] More in-depth study on the crystallization rule for CHAp will be performed in future works.

Conclusions

We fabricated different forms of nanocrystalline CHAp, such as microrods, sheet-like-assembled flowers, shaft wheel-like structures, bur-like spheres, dumbbell-shaped structures, and microspheres arrays at hydrothermal conditions by controlling pH in phosphate-surplus precursor solutions. The morphology, size, and alignment of CHAp nanoforms could be controlled by varying different experimental parameters, such as synthesis acidity, time, and HMT presence. In the crystallization process, the effect of the gradual release of OH^- from HMT is vital to regulate the nucleation and crystal growth of the 3D-structured CHAp flower crystal. The ability to design carbonated apatites will open up a wider choice of materials for use in biomedical implants, catalysts and environmental engineering.

Acknowledgements

This work was supported by the National Natural Science Foundation of China (nos. 21201142/51203028) and the basic research project of Sichuan Province for Science and Technology Development (No. 2015JY0147).

References

1 O. Altuntasoglu, Y. Matsuda, S. Ida and Y. Matsumoto, *Chem. Mater.*, 2010, **22**, 3158-3164.
2 B. W. Jacobs, M. A. Crimp, K. McElroy and V. M. Ayres, *Nano Lett.*, 2008, **8**, 4353-4358.
3 S. Rackauskas, H. Jiang, J. B. Wagner, S. D. Shandakov, T. W. Hansen, E. I. Kauppinen and A. G. Nasibulin, *Nano Lett.*, 2014, **14**, 5810-5813.
4 F. Gao, Q. Lu, X. Meng and S. Komarneni, *J. Phys. Chem. C*, 2008, **112**, 13359-13365.
5 D. Wang, D. Li, L. Guo, F. Fu, Z. Zhang and Q. Wei, *J. Phys. Chem. C*, 2009, **113**, 5984-5990.
6 J. Liu, Q. Wu and Y. Ding, *Eur. J. Inorg. Chem.*, 2005, **2005**, 4145-4149.
7 M. Aizawa, A. E. Porter, S. M. Best and W. Bonfield, *Biomaterials*, 2005, **26**, 3427-3433.
8 A. Ethirajan, U. Ziener, A. Chuvilin, U. Kaiser, H. Cölfen and K. Landfester, *Adv. Funct. Mater.*, 2008, **18**, 2221-2227.
9 C. Lai, S. Tang, Y. Wang and K. Wei, *Mater. Lett.*, 2005, **59**, 210-214.
10 J. Liu, K. Li, H. Wang, M. Zhu and H. Yan, *Chem. Phys. Lett.*, 2004, **396**, 429-432.
11 M. Jevtić, M. Mitrić, S. Škapin, B. Jančar, N. Ignjatović and D. Uskoković, *Cryst. Growth Des.*, 2008, **8**, 2217-2222.
12 C. Li, A.-K. Born, T. Schweizer, M. Zenobi-Wong, M. Cerruti and R. Mezzenga, *Adv. Mater.*, 2014, **26**, 3206-3206.
13 C.-M. Ho, W.-Y. Yu and C.-M. Che, *Angew. Chem. Int. Ed.*, 2004, **43**, 3303-3307.
14 B. Palazzo, M. Iafisco, M. Laforgia, N. Margiotta, G. Natile, C. L. Bianchi, D. Walsh, S. Mann and N. Roveri, *Adv. Funct. Mater.*, 2007, **17**, 2180-2188.
15 L.-X. Yang, J.-J. Yin, L.-L. Wang, G.-X. Xing, P. Yin and Q.-W. Liu, *Ceram. Int.*, 2012, **38**, 495-502.
16 J. Oliva, J. Cama, J. L. Cortina, C. Ayora and J. De Pablo, *J. Hazard. Mater.*, 2012, **213–214**, 7-18.
17 D. Snihirova, S. V. Lamaka, M. Taryba, A. N. Salak, S. Kallip, M. L. Zheludkevich, M. G. S. Ferreira and M. F. Montemor, *Acs Appl. Mater. Interfaces*, 2010, **2**, 3011-3022.

CrystEngComm Accepted Manuscript

18 X. Wang, J. Zhuang, Q. Peng and Y. D. Li, *Adv. Mater.*, 2006, **18**, 2031-2034.
19 L. Hao, H. Yang, N. Zhao, C. Du and Y. Wang, *Powder Technol.*, 2014, **253**, 172-177.
20 M.-G. Ma and J.-F. Zhu, *Eur. J. Inorg. Chem.*, 2009, **2009**, 5522-5526.
21 W. Amer, K. Abdelouahdi, H. R. Ramananarivo, M. Zahouily, A. Fihri, K. Djessas, K. Zahouily, R. S. Varma and A. Solhy, *CrystEngComm*, 2014, **16**, 543-549.
22 K. Lin, J. Chang, X. Liu, L. Chen and Y. Zhou, *CrystEngComm*, 2011, **13**, 4850-4855.
23 H. Ito, Y. Oaki and H. Imai, *Cryst. Growth Des.*, 2008, **8**, 1055-1059.
24 J. Zhan, Y. H. Tseng, J. C. C. Chan and C. Y. Mou, *Adv. Funct. Mater.*, 2005, **15**, 2005-2010.
25 A. Lak, M. Mazloumi, M. Mohajerani, A. Kajbafvala, S. Zanganeh, H. Arami and S. K. Sadrnezhaad, *J. Am. Ceram. Soc.*, 2008, **91**, 3292-3297.
26 H. Arce, M. L. Montero, A. Sáenz and V. M. Castaño, *Polyhedron*, 2004, **23**, 1897-1901.
27 R. Zhu, R. Yu, J. Yao, D. Wang and J. Ke, *J. Alloy. Compd.*, 2008, **457**, 555-559.
28 O. Kaygili, T. Ates, S. Keser, A. A. Al-Ghamdi and F. Yakuphanoglu, *Spectrochimica Acta Part A: Molecular and Biomolecular Spectroscopy*, 2014, **129**, 268-273.
29 K. Govender, D. S. Boyle, P. B. Kenway and P. O'Brien, *J. Mater. Chem.*, 2004, **14**, 2575-2591.
30 Y. Xu, J. Jiang, Y. Lu, R.-J. Sun, J. Song, L. Ren and S.-H. Yu, *Cryst. Growth Des.*, 2008, **8**, 3822-3828.
31 J. M. Delgado-López, M. Iafisco, I. Rodríguez, A. Tampieri, M. Prat and J. Gómez-Morales, *Acta Biomaterialia*, 2012, **8**, 3491-3499.
32 J. Gómez-Morales, J. M. Delgado-López, M. Iafisco, A. Hernández-Hernández and M. Prat, *Cryst. Growth Des.*, 2011, **11**, 4802-4809.
33 R. Boistelle and J. P. Astier, *J. Cryst. Growth*, 1988, **90**, 14-30.
34 D. Kashchiev and G. M. van Rosmalen, *Cryst. Res. Technol.*, 2003, **38**, 555-574.
35 E. Garskaite, K.-A. Gross, S.-W. Yang, T. C.-K. Yang, J.-C. Yang and A. Kareiva, *CrystEngComm*, 2014, **16**, 3950-3959.
36 J. D. B. Featherstone, S. Pearson and R. Z. LeGeros, *Caries Res.*, 1984, **18**, 63-66.
37 A. Hu, M. Li, C. Chang and D. Mao, *Journal of Molecular Catalysis A: Chemical*, 2007, **267**, 79-85.
38 T. Suzuki, I. Kumeda, K. Teshima and S. Oishi, *Chem. Phys. Lett.*, 2006, **421**, 343-347.
39 T. Kobayashi, S. Ono, S. Hirakura, Y. Oaki and H. Imai, *CrystEngComm*, 2012, **14**, 1143-1149.
40 K. Lin, J. Chang, Y. Zhu, W. Wu, G. Cheng, Y. Zeng and M. Ruan, *Cryst. Growth Des.*, 2009, **9**, 177-181.
41 Y.-J. Wu, Y.-H. Tseng and J. C. C. Chan, *Cryst. Growth Des.*, 2010, **10**, 4240-4242.
42 H. Tlatlik, P. Simon, A. Kawska, D. Zahn and R. Kniep, *Angew. Chem. Int. Ed.*, 2006, **45**, 1905-1910.
43 T. Y. Olson, C. A. Orme, T. Y.-J. Han, M. A. Worsley, K. A. Rose, J. H. Satcher and J. D. Kuntz, *CrystEngComm*, 2012, **14**, 6384-6389.

CrystEngComm Accepted Manuscript

CHAp powders with controllable morphologies and sizes were synthesized using HMT as a hydroxide anion-generating agent in a phosphate-surplus solution.

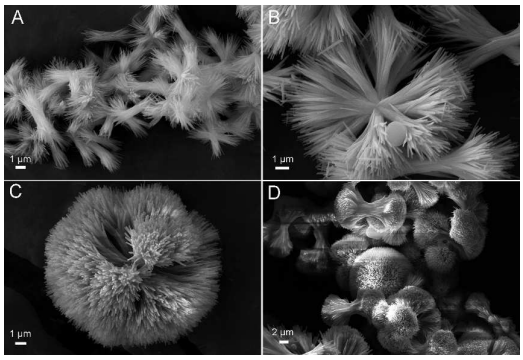

CrystEngComm Accepted Manuscript